Available online at www.sciencedirect.com
ScienceDirect
Ceramics International 35 (2009) 1145–1150
CERAMICS INTERNATIONAL
www.elsevier.com/locate/ceramint

Electrochemical properties of $LiNi_{1-y}M_yO_2$ (M = Ni, Ga, Al and/or Ti) cathodes

MyoungYoup Song [a,*], ChangKee Park [b], SoonDo Yoon [c], HyeRyoung Park [c], Daniel R. Mumm [d]

[a] Division of Advanced Materials Engineering, Nanomaterials Processing Research Center, Engineering Research Institute, Chonbuk National University, 664-14 1ga Deogjindong Deogjingu, Jeonju 561-756, Republic of Korea
[b] Graduate School, Department of Materials Engineering, Chonbuk National University, 664-14 1ga Deogjindong Deogjingu, Jeonju 561-756, Republic of Korea
[c] School of Applied Chemical Engineering, Chonnam National University, 300 Yongbongdong Bukgu, Gwangju 500-757, Republic of Korea
[d] Department of Chemical Engineering and Materials Science, University of California, Irvine, CA 92697-2575, USA

Received 27 March 2008; received in revised form 16 April 2008; accepted 20 May 2008
Available online 25 July 2008

Abstract

$LiNi_{1-y}M_yO_2$ specimens with compositions $LiNiO_2$, $LiNi_{0.975}Ga_{0.025}O_2$, $LiNi_{0.975}Al_{0.025}O_2$, $LiNi_{0.995}Ti_{0.005}O_2$ and $LiNi_{0.990}Al_{0.005}Ti_{0.005}O_2$ were synthesized by wet milling and solid-state reaction, in which the mixtures with these compositions were preheated at 450 °C for 5 h in air, pressed into pellets and calcined at 750 °C for 30 h under an oxygen stream. All the synthesized samples possessed the α-$NaFeO_2$ structure of the rhombohedral system (space group; $R\bar{3}m$) with no evidence of any impurities. Among all the specimens, $LiNi_{0.990}Al_{0.005}Ti_{0.005}O_2$ has the largest first discharge capacity 196.3 mAh/g at a rate of 0.1*C*. $LiNiO_2$ has the best cycling performance, its degradation rate of discharge capacity being 1.06 mAh/(g cycle).
© 2008 Elsevier Ltd and Techna Group S.r.l. All rights reserved.

Keywords: $LiNi_{1-y}M_yO_2$ (M = Ni, Ga, Al and/or Ti); Milling; Solid-state reaction method; Electrochemical properties; I_{003}/I_{104}; *R*-factor

1. Introduction

Transition metal oxides such as $LiMn_2O_4$ [1–3], $LiCoO_2$ [4–6] and $LiNiO_2$ [7–10] have been intensively investigated in order to use them as the cathode materials of lithium secondary batteries. $LiMn_2O_4$ is comparatively inexpensive and does not bring about any environmental pollution, but its cycling performance is not adequate. $LiCoO_2$ has a large diffusivity and a high operating voltage, and it can be easily prepared. However, it has the disadvantage that it contains Co, an expensive element. $LiNiO_2$ is a very promising cathode material since it has a large discharge capacity [11] and is excellent from the economic and environmental viewpoints. On the other hand, its preparation is very difficult compared with $LiCoO_2$ and $LiMn_2O_4$.

It is known that $Li_{1-x}Ni_{1+x}O_2$ forms rather than the stoichiometric $LiNiO_2$ during preparation [12] due to cation mixing. Excess nickel occupies the Li sites, destroying the ideally layered structure and preventing the lithium ions from undergoing the easy movement required for intercalation and deintercalation during cycling. This results in a small discharge capacity and poor cycling performance.

To improve the electrochemical properties of $LiNiO_2$, Co [13], Al [14,15], Ti [16,17], Ga [11], Mn [18] and Fe [19,20] were substituted for nickel by the synthesis in oxygen. Guilmard et al. [14] investigated the electrochemical performances of $LiNi_{1-y}Al_yO_2$ ($0.10 \leq y \leq 0.50$) specimens synthesized by a co-precipitation method. They showed that aluminum substitution suppressed all the phase transitions observed for the $LiNiO_2$ system. According to Gao et al. [16], the substitution of Ti for Ni resulted in a large discharge capacity and good cycling performance. Chang et al. [17] detected partial disordering between the transition metal (Ni and Ti) layer and lithium by Rietveld refinement in $Li_xNi_{1-y}Ti_yO_2$ ($0.1 \leq y \leq 0.5$) prepared

* Corresponding author. Tel.: +82 63 270 2379; fax: +82 63 270 2386.
E-mail address: songmy@chonbuk.ac.kr (M. Song).

0272-8842/$34.00 © 2008 Elsevier Ltd and Techna Group S.r.l. All rights reserved.
doi:10.1016/j.ceramint.2008.05.015

by solid-state reaction. By considering the ionic radius and the Ni–O bond length, they concluded that the Ni(II) ions are partially stabilized in the lithium sites. Nishida et al. [11] reported that gallium-doping into $LiNiO_2$ stabilizes the crystal structure during the charging process and leads to better cycling performance than $LiNiO_2$.

In this work, $LiNi_{1-y}M_yO_2$ (M = Ni, Ga, Al and/or Ti) specimens were synthesized by milling and solid-state reaction, and the electrochemical properties of the synthesized samples were investigated.

2. Materials and methods

$LiNi_{1-y}M_yO_2$ specimens with compositions $LiNiO_2$, $LiNi_{0.975}Ga_{0.025}O_2$, $LiNi_{0.975}Al_{0.025}O_2$ and $LiNi_{0.995}Ti_{0.005}O_2$, $LiNi_{0.990}Al_{0.005}Ti_{0.005}O_2$ were synthesized by milling and solid-state reaction. These compositions were chosen because the specimens with these compositions had relatively good electrochemical properties in our previous works [21,22]. $LiOH{\cdot}H_2O$ (Kojundo Chemical Lab. Co., Ltd., purity 99%), $Ni(OH)_2$ (Kojundo Chemical Lab. Co., Ltd., purity 99.9%), Ga_2O_3 (Aldrich Chemical, purity 99%), $Al(OH)_3$ (Kojundo Chemical Lab. Co., Ltd., purity 99.99%) and TiO_2 (Aldrich Chemical, purity 99%) were used as the starting materials. These were mechanically mixed by wet SPEX milling under distilled acetone for 1 h, and dried in a shaking incubator with 50 rpm at 50 °C for 48 h. The mixtures were then preheated at 450 °C for 5 h in air, pressed into pellets and calcined at 750 °C for 30 h under an oxygen stream. The phase identification of the synthesized samples was carried out by the X-ray powder diffraction analysis (Rigaku III/A diffractometer) using Cu Kα radiation, scanning rate of 6° min^{-1} and 2θ of $10^\circ \leq 2\theta \leq 80^\circ$. The electrochemical cells consisted of $LiNi_{1-y}M_yO_2$ as a positive electrode, Li foil as a negative electrode and an electrolyte [Purelyte (Samsung General Chemicals Co., Ltd.)] prepared by dissolving 1 M $LiPF_6$ in a 1:1 (volume ratio) mixture of ethylene carbonate (EC) and diethyl carbonate (DEC). The positive electrode consisted of 85 wt.% synthesized materials, 10 wt.% acetylene black and 5 wt.% polyvinylidene fluoride (PVDF) binder dissolved in 1-methyl-2-pyrrolidinone (NMP). A Whatman glass-filter was used as a separator. The coin-type (2016) cells were assembled in an argon-filled dry box. All of the electrochemical tests were performed at room temperature with a potentiostatic/galvanostatic system. The cells were cycled between 2.7 and 4.4 V at a rate of 0.1*C*.

Fig. 1 shows the experimental procedure for the $LiNi_{1-y}M_yO_2$ electrodes prepared by the solid-state reaction method after milling.

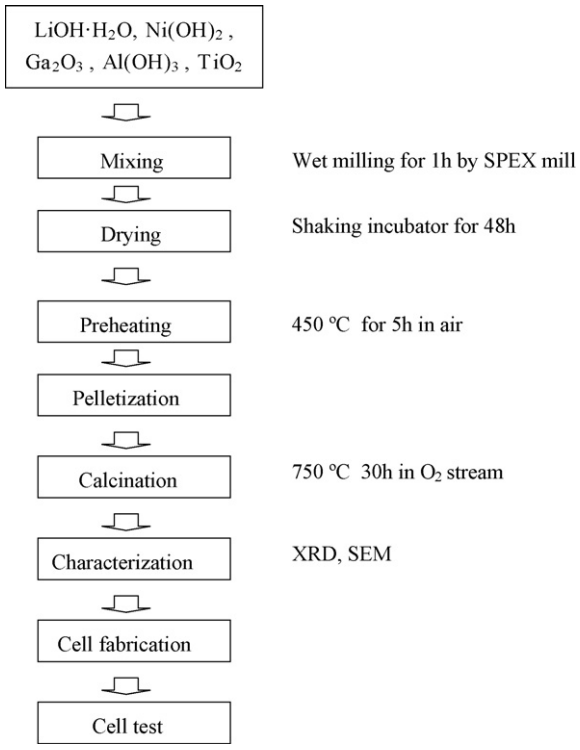

Fig. 1. Experimental procedure for $LiNi_{1-y}M_yO_2$ electrode prepared by the solid-state reaction method after milling.

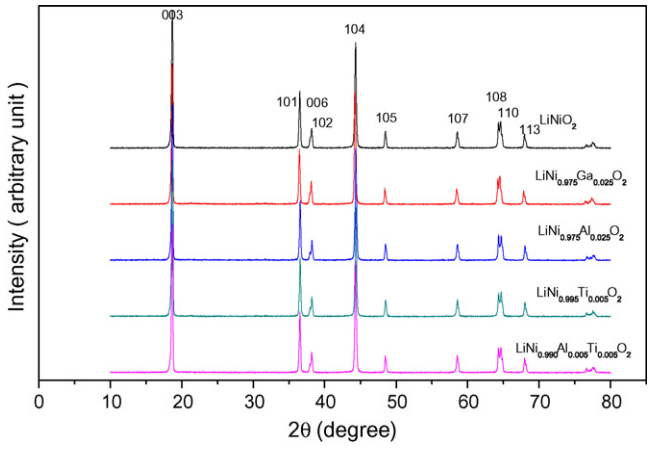

Fig. 2. XRD patterns of the samples calcined at 750 °C for 30 h in O_2 stream (after milling for 1 h and preheating in air at 450 °C for 5 h).

3. Results and discussion

Fig. 2 shows the XRD patterns of the samples $LiNiO_2$, $LiNi_{0.975}Ga_{0.025}O_2$, $LiNi_{0.975}Al_{0.025}O_2$, $LiNi_{0.995}Ti_{0.005}O_2$ and $LiNi_{0.990}Al_{0.005}Ti_{0.005}O_2$ calcined at 750 °C for 30 h in O_2 stream (after milling for 1 h and preheating in air at 450 °C for 5 h). All the samples possess the α-$NaFeO_2$ structure of the rhombohedral system (space group; $R\bar{3}m$) with no evidence of any impurities. The $R\bar{3}m$ structure is distorted in the *c*-axis direction of the hexagonal structure. This is reflected by the split of the 0 0 6 and 1 0 2 peaks and of the 1 0 8 and 1 1 0 peaks in the XRD patterns. The 1 0 8 and 1 1 0 peaks were split for all of the samples.

Ohzuku et al. [23] reported that electrochemically reactive $LiNiO_2$ showed a larger integrated intensity ratio of the 0 0 3 peak to the 1 0 4 peak (I_{003}/I_{104}) and a clear split of the 1 0 8 and 1 1 0 peaks in its XRD patterns. The degree of cation mixing (displacement of nickel and lithium ions) is low if the value of I_{003}/I_{104} is large and the 1 0 8 and 1 1 0 peaks are split clearly. The value of $(I_{006} + I_{102})/I_{101}$, called the *R*-factor, is known to decrease as the unit cell volume of $Li_yNi_{2-y}O_2$ decreases. The

Table 1
Data calculated from XRD patterns of the samples calcined at 750 °C for 30 h in O_2 stream (after milling for 1 h and preheating in air at 450 °C for 5 h)

	a (Å)	c (Å)	c/a	I_{003}/I_{104}	R-factor	Unit cell volume (Å^3)
$LiNiO_2$	2.876	14.253	4.956	1.31	0.36	102.09
$LiNi_{0.975}Ga_{0.025}O_2$	2.885	14.255	4.941	1.25	0.43	102.75
$LiNi_{0.975}Al_{0.025}O_2$	2.874	14.252	4.959	1.39	0.47	101.95
$LiNi_{0.995}Ti_{0.005}O_2$	2.877	14.239	4.949	1.43	0.47	102.07
$LiNi_{0.990}Al_{0.005}Ti_{0.005}O_2$	2.876	14.254	4.956	1.33	0.33	102.10

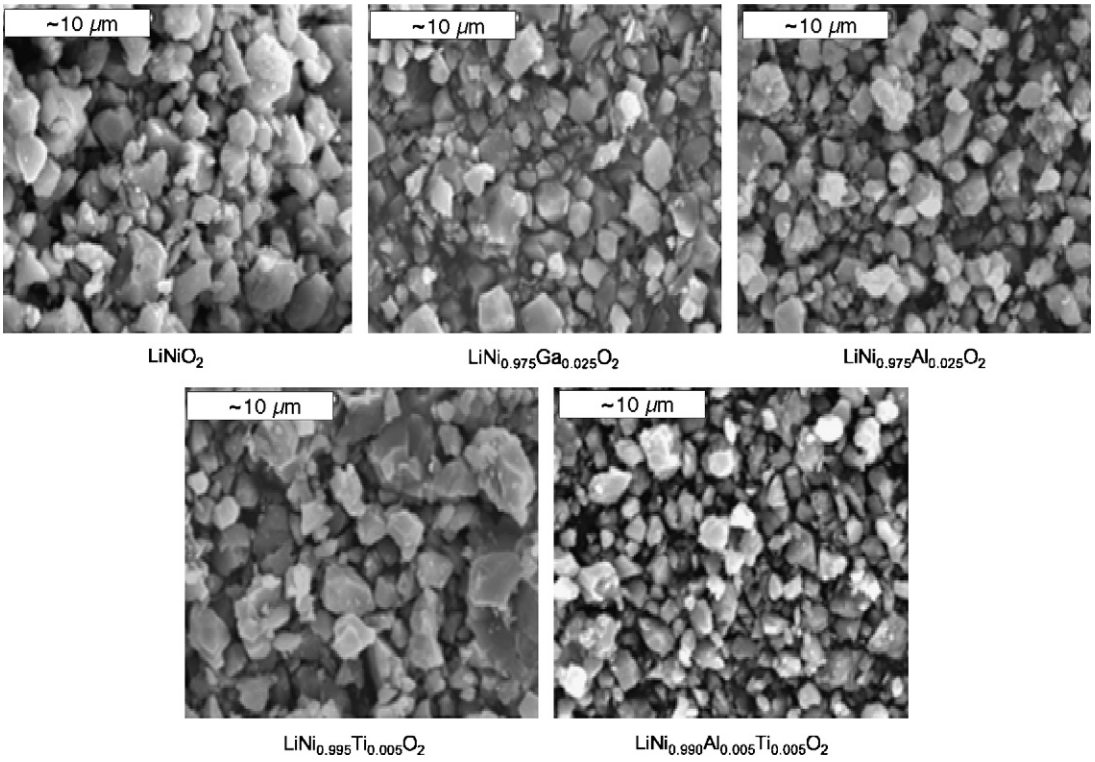

Fig. 3. Microstructures observed by SEM of the samples calcined at 750 °C for 30 h in O_2 stream (after milling for 1 h and preheating in air at 450 °C for 5 h).

R-factor increases as y in $Li_yNi_{2-y}O_2$ decreases for y near 1. This indicates that the R-factor increases as the degree of cation mixing becomes larger [7].

Table 1 shows the values of a, c, c/a, I_{003}/I_{104}, R-factor, unit cell volume calculated from XRD patterns of the samples calcined at 750 °C for 30 h in O_2 stream (after milling for 1 h and preheating in air at 450 °C for 5 h). $LiNi_{0.995}Ti_{0.005}O_2$ has the largest value of I_{003}/I_{104} and its value decreases in the order of $LiNi_{0.975}Al_{0.025}O_2$, $LiNi_{0.990}Al_{0.005}Ti_{0.005}O_2$, $LiNiO_2$ and $LiNi_{0.975}Ga_{0.025}O_2$. $LiNi_{0.990}Al_{0.005}Ti_{0.005}O_2$ has the smallest value of R-factor and its value increases in the order of $LiNiO_2$, $LiNi_{0.975}Ga_{0.025}O_2$, $LiNi_{0.975}Al_{0.025}O_2$ and $LiNi_{0.995}Ti_{0.005}O_2$.

Fig. 3 shows the microstructures observed by SEM of the samples calcined at 750 °C for 30 h in O_2 stream (after milling for 1 h and preheating in air at 450 °C for 5 h). $LiNi_{0.995}Ti_{0.005}O_2$ has the largest particles and the particle size decreases in the order of $LiNiO_2$, $LiNi_{0.975}Ga_{0.025}O_2$, $LiNi_{0.975}Al_{0.025}O_2$ and $LiNi_{0.990}Al_{0.005}Ti_{0.005}O_2$. $LiNi_{0.975}Al_{0.025}O_2$ and $LiNi_{0.990}Al_{0.005}Ti_{0.005}O_2$ have a little more homogeneous particle sizes compared with the other samples.

Fig. 4 shows the variations of the plot discharge capacity vs. number of cycles n at a rate of 0.1C for $LiNiO_2$, $LiNi_{0.975}Ga_{0.025}O_2$, $LiNi_{0.975}Al_{0.025}O_2$, $LiNi_{0.995}Ti_{0.005}O_2$ and $LiNi_{0.990}Al_{0.005}Ti_{0.005}O_2$. $LiNi_{0.990}Al_{0.005}Ti_{0.005}O_2$ has the largest first discharge capacity 196.3 mAh/g, and those of $LiNiO_2$, $LiNi_{0.975}Ga_{0.025}O_2$, $LiNi_{0.975}Al_{0.025}O_2$ and $LiNi_{0.995}Ti_{0.005}O_2$

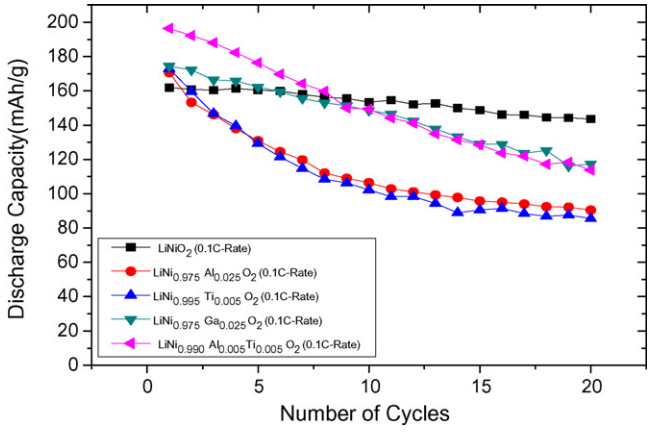

Fig. 4. Variations of the plot discharge capacity vs. number of cycles at 0.1C rate for $LiNiO_2$, $LiNi_{0.975}Ga_{0.025}O_2$, $LiNi_{0.975}Al_{0.025}O_2$, $LiNi_{0.995}Ti_{0.005}O_2$ and $LiNi_{0.990}Al_{0.005}Ti_{0.005}O_2$.

were 161.8, 174.4, 170.5 and 172.9 mAh/g, respectively. At $n = 20$ $LiNiO_2$ has the largest discharge capacity, 143.5 mAh/g, and those of $LiNi_{0.975}Ga_{0.025}O_2$, $LiNi_{0.975}Al_{0.025}O_2$, $LiNi_{0.995}Ti_{0.005}O_2$ and $LiNi_{0.990}Al_{0.005}Ti_{0.005}O_2$ were 117.4, 90.5, 85.5 and 113.8 mAh/g, respectively. $LiNiO_2$ has the best cycling performance and its degradation rate of discharge capacity being 1.06 mAh/(g cycle) between the first cycle and the 20th cycle.

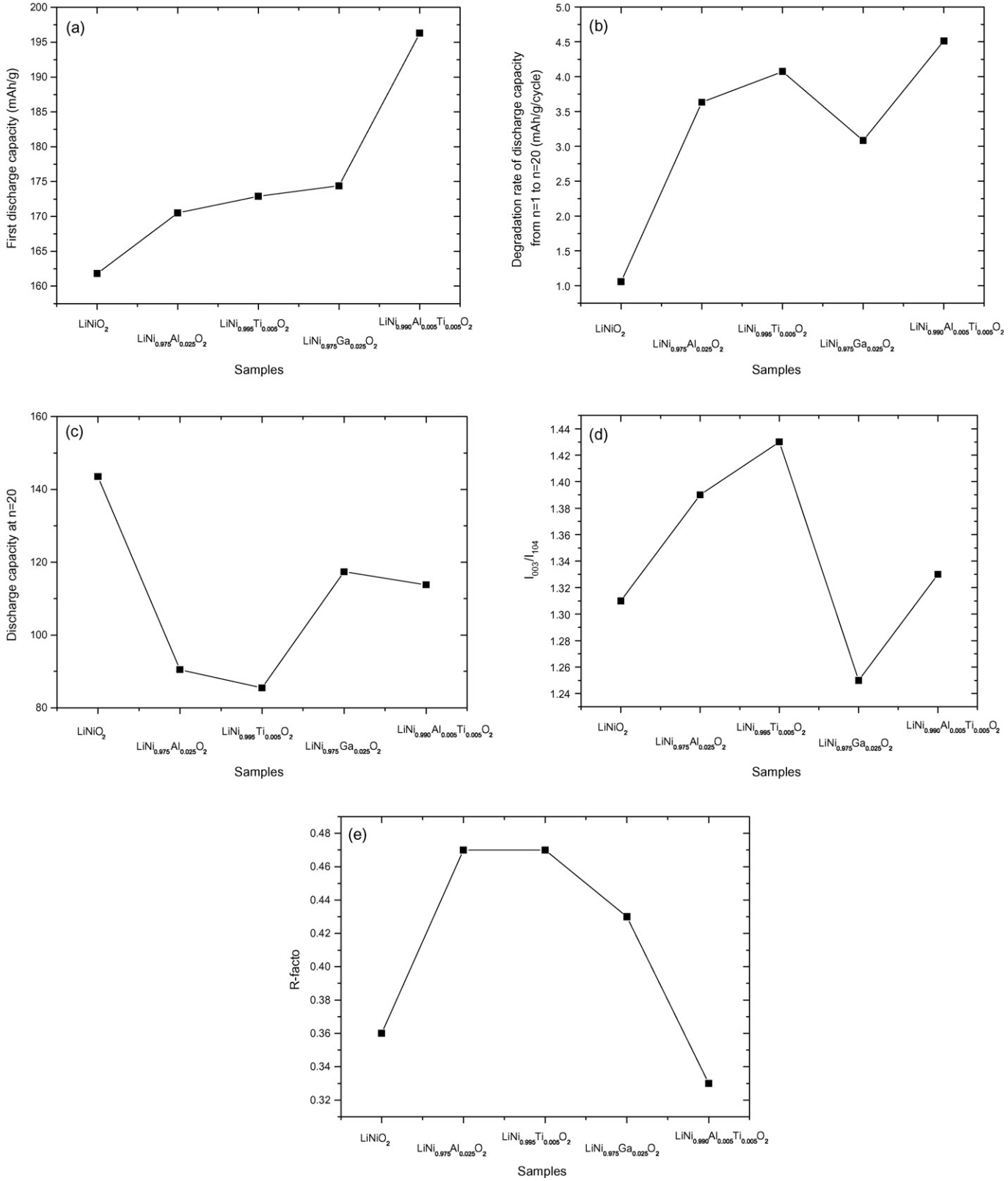

Fig. 5. Variations of the first discharge capacity (a) and the degradation rate of discharge capacity from $n = 1$ to $n = 20$ (b) at a rate of $0.1C$ with the samples $LiNiO_2$, $LiNi_{0.975}Al_{0.025}O_2$, $LiNi_{0.995}Ti_{0.005}O_2$, $LiNi_{0.975}Ga_{0.025}O_2$ and $LiNi_{0.990}Al_{0.005}Ti_{0.005}O_2$.

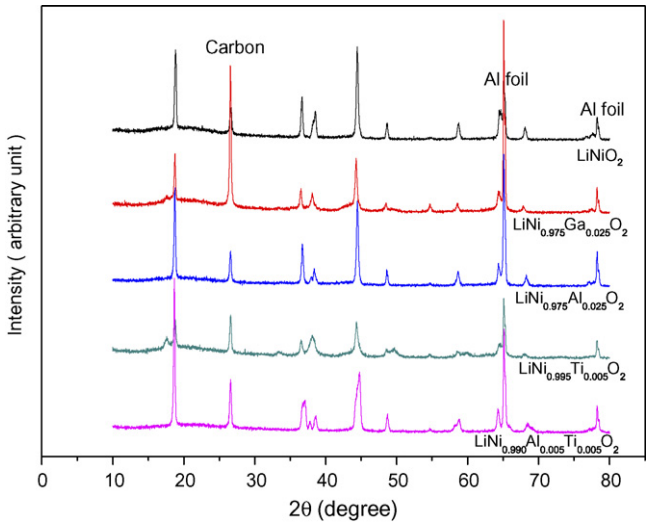

Fig. 6. XRD patterns of the samples $LiNiO_2$, $LiNi_{0.975}Ga_{0.025}O_2$, $LiNi_{0.975}Al_{0.025}O_2$, $LiNi_{0.995}Ti_{0.005}O_2$ and $LiNi_{0.990}Al_{0.005}Ti_{0.005}O_2$ after 50 charge–discharge cycles.

Fig. 5 shows variations of (a) the first discharge capacity, (b) the degradation rate of discharge capacity from $n = 1$ to $n = 20$, (c) the discharge capacity at $n = 20$ at a rate of $0.1C$, (d) I_{003}/I_{104} and (e) R-factor with the samples $LiNiO_2$, $LiNi_{0.975}Al_{0.025}O_2$, $LiNi_{0.995}Ti_{0.005}O_2$, $LiNi_{0.975}Ga_{0.025}O_2$ and $LiNi_{0.990}Al_{0.005}Ti_{0.005}O_2$. The capacity degradation rates were calculated from the discharge capacities between the first and the 20th discharge cycles. The first discharge capacity increases along with the samples $LiNiO_2$, $LiNi_{0.975}Al_{0.025}O_2$, $LiNi_{0.995}Ti_{0.005}O_2$, $LiNi_{0.975}Ga_{0.025}O_2$ and $LiNi_{0.990}Al_{0.005}Ti_{0.005}O_2$. The degradation rate of discharge capacity increases roughly in the above order of the samples. This indicates that the sample with a large first discharge capacity shows a high degradation rate of discharge capacity. The variation of the discharge capacity at $n = 20$ is roughly inverse to that of R-factor. This shows that the sample with a lower degree of cation mixing (a smaller R-factor) shows a higher discharge capacity at $n = 20$.

Fig. 6 shows the XRD patterns of the samples $LiNiO_2$, $LiNi_{0.975}Ga_{0.025}O_2$, $LiNi_{0.975}Al_{0.025}O_2$, $LiNi_{0.995}Ti_{0.005}O_2$ and $LiNi_{0.990}Al_{0.005}Ti_{0.005}O_2$ after 50 charge–discharge cycles. All the samples possess the α-$NaFeO_2$ structure of the rhombohedral system (space group; $R\bar{3}m$), and the peaks of acetylene black (carbon) and Al foil are also observed.

Table 2 gives the values of a, c, c/a, I_{003}/I_{104}, R-factor and unit cell volume calculated from the XRD patterns of the samples $LiNiO_2$, $LiNi_{0.975}Ga_{0.025}O_2$, $LiNi_{0.975}Al_{0.025}O_2$, $LiNi_{0.995}Ti_{0.005}O_2$ and $LiNi_{0.990}Al_{0.005}Ti_{0.005}O_2$ after 50 charge–discharge cycles. $LiNi_{0.990}Al_{0.005}Ti_{0.005}O_2$ has the largest value of I_{003}/I_{104} and its value decreases in the order of $LiNi_{0.975}Al_{0.025}O_2$, $LiNi_{0.975}Ga_{0.025}O_2$, $LiNiO_2$ and $LiNi_{0.995}Ti_{0.005}O_2$. $LiNi_{0.975}Al_{0.025}O_2$ has the smallest value of R-factor and its value increases in the order of $LiNi_{0.990}Al_{0.005}Ti_{0.005}O_2$, $LiNi_{0.975}Ga_{0.025}O_2$, $LiNiO_2$ and $LiNi_{0.995}Ti_{0.005}O_2$. After 50 charge–discharge cycles most of the I_{003}/I_{104} values of the samples decreased and all the R-factor values increased, as compared with those of the as-prepared samples.

Fig. 7 Microstructures observed by SEM of the samples $LiNiO_2$, $LiNi_{0.975}Ga_{0.025}O_2$, $LiNi_{0.975}Al_{0.025}O_2$, $LiNi_{0.995}Ti_{0.005}O_2$ and $LiNi_{0.990}Al_{0.005}Ti_{0.005}O_2$ after 50 charge–

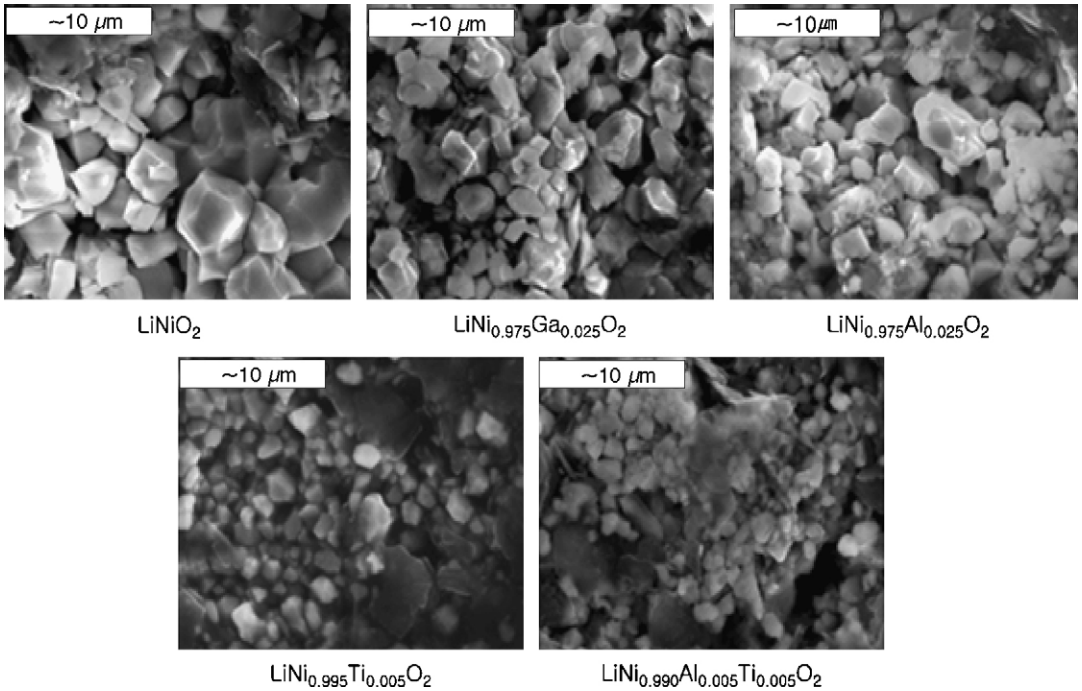

Fig. 7. Microstructures observed by SEM of the samples $LiNiO_2$, $LiNi_{0.975}Ga_{0.025}O_2$, $LiNi_{0.975}Al_{0.025}O_2$, $LiNi_{0.995}Ti_{0.005}O_2$ and $LiNi_{0.990}Al_{0.005}Ti_{0.005}O_2$ after 50 charge–discharge cycles.

Table 2
Values of a, c, c/a, I_{003}/I_{104}, R-factor and unit cell volume calculated from XRD patterns of the samples after 50 charge–discharge cycles

	a (Å)	c (Å)	c/a	I_{003}/I_{104}	R-factor	Unit cell volume (Å^3)
$LiNiO_2$	2.880	14.119	4.902	0.87	1.07	101.42
$LiNi_{0.975}Ga_{0.025}O_2$	2.888	14.166	4.905	0.94	0.99	102.32
$LiNi_{0.975}Al_{0.025}O_2$	2.872	14.179	4.959	1.10	0.53	101.28
$LiNi_{0.995}Ti_{0.005}O_2$	2.889	14.164	4.937	0.78	2.30	102.38
$LiNi_{0.990}Al_{0.005}Ti_{0.005}O_2$	2.886	14.239	4.934	1.71	0.86	102.70

discharge cycles. $LiNiO_2$ has the largest particle size, and the particle size decreases in the order of $LiNi_{0.975}Al_{0.025}O_2$, $LiNi_{0.975}Ga_{0.025}O_2$, $LiNi_{0.995}Ti_{0.005}O_2$ and $LiNi_{0.990}Al_{0.005}Ti_{0.005}O_2$. $LiNi_{0.975}Ga_{0.025}O_2$ and $LiNi_{0.975}Al_{0.025}O_2$ have a little more homogeneous particle sizes, compared with the other samples.

4. Conclusions

$LiNi_{1-y}M_yO_2$ specimens with compositions $LiNiO_2$, $LiNi_{0.975}Ga_{0.025}O_2$, $LiNi_{0.975}Al_{0.025}O_2$, $LiNi_{0.995}Ti_{0.005}O_2$, $LiNi_{0.990}Al_{0.005}Ti_{0.005}O_2$ were synthesized by wet milling and solid-state reaction. All the synthesized samples possessed the α-$NaFeO_2$ structure of the rhombohedral system (space group; $R\bar{3}m$) with no evidence of any impurities. Among all the specimens, $LiNi_{0.990}Al_{0.005}Ti_{0.005}O_2$ has the largest first discharge capacity 196.3 mAh/g at a rate of $0.1C$. At $n = 20$ $LiNiO_2$ has the largest discharge capacity, 143.5 mAh/g. $LiNiO_2$ has the best cycling performance, its degradation rate of discharge capacity being 1.06 mAh/g/cycle. After 50 charge–discharge cycles most of the I_{003}/I_{104} values of the samples decreased and all the R-factor values increased, as compared with those of the as-prepared samples.

Acknowledgement

This work was supported by grant No. R01-2003-000-10325-0 from the Basic Research Program of the Korea Science & Engineering Foundation.

References

[1] J.M. Tarascon, E. Wang, F.K. Shokoohi, W.R. McKinnon, S. Colson, J. Electrochem. Soc. 138 (1991) 2859.
[2] A.R. Armstrong, P.G. Bruce, Lett. Nat. 381 (1996) 499.
[3] M.Y. Song, D.S. Ahn, Solid State Ionics 112 (1998) 245.
[4] K. Ozawa, Solid State Ionics 69 (1994) 212.
[5] R. Alcántara, P. Lavela, J.L. Tirado, R. Stoyanova, E. Zhecheva, J. Solid State Chem. 134 (1997) 265.
[6] Z.S. Peng, C.R. Wan, C.Y. Jiang, J. Power Sources 72 (1998) 215.
[7] J.R. Dahn, U. von Sacken, C.A. Michal, Solid State Ionics 44 (1990) 87.
[8] J.R. Dahn, U. von Sacken, M.R. Jukow, H. Aljanaby, J. Electrochem. Soc. 138 (1991) 2207.
[9] A. Marini, V. Massarotti, V. Berbenni, D. Capsoni, R. Riccardi, E. Antolini, B. Passalacqua, Solid State Ionics 45 (1991) 143.
[10] W. Ebner, D. Fouchard, L. Xie, Solid State Ionics 69 (1994) 238.
[11] Y. Nishida, K. Nakane, T. Stoh, J. Power Sources 68 (1997) 561.
[12] J. Morales, C. Perez-Vicente, J.L. Tirado, Mater. Res. Bull. 25 (1990) 623.
[13] A. Rougier, I. Saadoune, P. Gravereau, P. Willmann, C. Delmas, Solid State Ionics 90 (1996) 83.
[14] M. Guilmard, A. Rougier, M. Grune, L. Croguennec, C. Delmas, J. Power Sources 115 (2003) 305.
[15] M.Y. Song, R. Lee, I.H. Kwon, Solid State Ionics 156 (2003) 319.
[16] Y. Gao, M.V. Yakovleva, W.B. Ebner, Electrochem. Soc. 142 (1995) 702.
[17] S.H. Chang, S.G. Kang, S.W. Song, J.B. Yoon, J.H. Choy, Solid State Ionics 86–88 (1996) 171.
[18] M. Guilmard, L. Croguennec, C. Delmas, J. Electrochem. Soc. 150 (10) (2003) A1287.
[19] J.N. Reimers, E. Rossen, C.D. Jones, J.R. Dahn, Solid State Ionics 61 (1993) 335.
[20] R. Kanno, T. Shirane, Y. Inaba, Y. Kawamoto, J. Power Sources 68 (1997) 145.
[21] H.U. Kim, S.D. Youn, J.C. Lee, H.R. Park, C.G. Park, M.Y. Song, J. Kor. Ceram. Soc. 42 (9) (2005) 631.
[22] H.U. Kim, S.D. Youn, J.C. Lee, H.R. Park, M.Y. Song, J. Kor. Ceram. Soc 42 (5) (2005) 352.
[23] T. Ohzuku, A. Ueda, M. Nagayana, J. Electrochem. Soc. 140 (1993) 1862.